




Enhancing weak-magnetic-field sensing of a cavity-magnon system with dual frequency modulationZheng Liu , Yu-qiang Liu, Zi-yi Mai , Yi-jia Yang, Nan-nan Zhou, and Chang-shui Yu **School of Physics, Dalian University of Technology, Dalian 116024, People's Republic of China*

(Received 18 July 2023; revised 19 September 2023; accepted 22 January 2024; published 12 February 2024)

The crucial limitation of improving the sensitivity of the detection of weak magnetic fields is the unavoidable measurement noise. In this paper, we propose a scheme to achieve precise sensing robust against additional noise by employing a dual frequency bias field modulation within a cavity-magnon system. We find that the antirotating wave term can amplify the signal of the detected magnetic field, but this amplification effect must coexist with the rotating wave term. In particular, by the bias field modulation, we find the robustness against cavity field thermal noise is substantially enhanced, quantum noise and cavity field thermal noise is greatly reduced, and the external magnetic field signal is amplified, thereby improving the weak-magnetic-field sensing system's sensitivity. Compared with the previous scheme, our scheme requires neither an ultrastrong- or deep-strong-coupling mechanism nor the suppression of the additional noise by increasing the electromagnetic cooperativity. Our scheme could provide a valuable candidate for weak-magnetic-field sensing.

DOI: [10.1103/PhysRevA.109.023709](https://doi.org/10.1103/PhysRevA.109.023709)**I. INTRODUCTION**

The precise measurement of weak magnetic fields is currently a major topic of interest in both theory and experiment [1–7] which is widely applied in geophysics [8], biology [9,10], and dark matter search [11]. Many magnetometers with certain operating frequencies and environments, such as superconducting quantum interference magnetometers (SQUIDs) [12], atomic magnetometers [13], and nitrogen-vacancy centers magnetometers [14], have been extensively studied. How to realize a weak-magnetic-field sensing with high sensitivity, wide frequency range, and noise immunity is attracting increasing interest.

Additional noise is the core factor limiting the detection sensitivity in quantum sensing [15], which, distinguished from probe noise, includes the quantum noise and thermal noise of the whole system except the probe. Over the past decade, many approaches have been proposed to reduce the quantum noise without thermal noise explicitly taken into account. For example, quantum noise is reduced in precision measurement and breaks the standard quantum limit (SQL) in optomechanical force sensing, such as coherent quantum noise cancellation (CQNC) [16–21], non-Markovian regime [22], squeezed cavity field [23–27], and so on. The mechanical oscillator's sensitivity to external forces and the unique optical readout in the cavity optomechanical system enables it to naturally detect weak force signals [28,29]. Therefore, if some systems have highly sensitive probes to measure external magnetic fields and the corresponding readout device, these systems can also be used for magnetic field sensing. and the above scheme for reducing quantum noise is also applicable to weak magnetic sensing.

Cavity-magnon systems, composed of a microwave cavity and yttrium iron garnet (YIG) sphere, have recently gained significant attention in addition to the cavity optomechanical systems [11,30–35]. The cavity-magnon system can serve as a feasible platform to investigate quantum magnetic field sensing in the field of quantum precision measurement. The reason is, on one hand, the YIG sphere is an excellent ferromagnetic material that produces a low-excitation magnon mode (Kittel mode) [36] with high spin density, low decay rate [37], and high-frequency tuning [38], which is beneficial to highly sensitive magnetic field sensing, and the microwave cavity, on the other hand, facilitates microwave readout and can achieve strong coupling or even ultrastrong coupling with the YIG sphere [39–42], making them ideal for various quantum information processing applications, such as the preparation of macroscopic Schrödinger cat states [43], steady-state magnon entanglement [44–48], and blockade of the magnon [49,50]. However, the sensing of weak magnetic fields using the cavity-magnon system remains challenged due to the presence of additional noise, i.e., quantum noise and microwave cavity field thermal noise. Even though the ultrastrong or deep-strong coupling allows the interaction of the antirotating wave, which can effectively suppress quantum noise and cavity field thermal noise below the SQL and amplify the signal [7], realizing the ultrastrong or deep-strong coupling *per se* is also more challenging than the realization of the strong coupling; additionally, what role the rotating wave and antirotating wave interactions play in weak-magnetic-field sensing remains unclear.

In this paper, to sense a weak-magnetic-field signal, we introduce a dual frequency bias magnetic field modulation to the cavity-magnon system with the YIG sphere coupling with a microwave cavity through dipole-dipole interaction [51]. The external magnetic field interacting with the YIG sphere affects the microwave output spectrum, which can be measured by the cavity field phase quadrature detection

*yqs@dlut.edu.cn

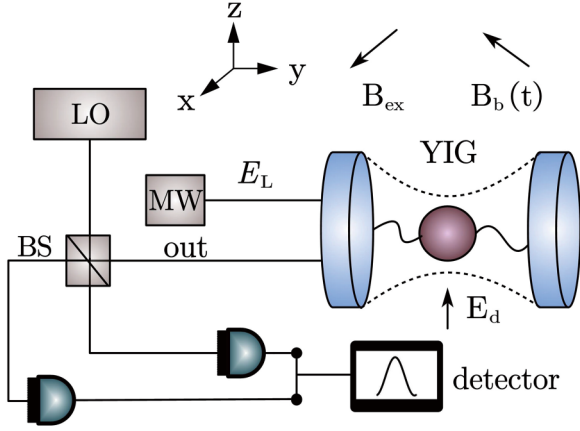


FIG. 1. The schematic diagram of a weak-magnetic-field sensing system. The YIG sphere is placed at the maximum value of the field generated by the microwave cavity, the time-dependent dual frequency modulation bias magnetic field $B_b(t)$ is along the x - z direction to regulate the frequency of the magnon mode, and the cavity field and magnon mode are driven by two classical pump fields, whose driving amplitudes are E_L and E_d , respectively. Detected magnetic field B_{ex} is assumed to be along the x direction. The information of the detected magnetic field is determined by the information of the output cavity field, and its output is analyzed by a balanced homodyne detector.

method. It is shown that the dual frequency bias magnetic field modulation can realize the antirotating wave interaction through the strong-coupling regime instead of the ultrastrong- or deep-strong-coupling regime. It can especially control the proportion of rotating and antirotating wave terms in the system which can reveal the roles of each type of interaction, by which we find that the antirotating wave term can amplify the detected field signal, but this amplification effect must coexist with the rotating wave term. We show that in our scheme, there exists a noise-resistant frequency band tolerating additional noise if selecting appropriate parameters. In particular, the sensitivity can be improved and the system's response

to weak magnetic fields can be amplified in this frequency band. Compared to the scheme achieving uncontrolled antirotating wave terms under ultrastrong- or deep-strong-coupling mechanisms [7], we find that our scheme can achieve additional noise suppression of the same order of magnitude under ultrastrong- or even deep-strong-coupling mechanisms. This only requires the cavity magnetic strong-coupling mechanism, which is of course more conducive to experimental implementation. Moreover, we can foresee that when our scheme is in the super-strong-coupling mechanism or deep-strong-coupling mechanism, the additional noise will be suppressed to a greater extent. The rest of the paper is organized as follows. In Sec. II, we introduce the specific model of our dual frequency modulation magnetic field sensing scheme and the derivation of the Hamiltonian. In Sec. III, we analyze the dissipative dynamics of the system and provide an analytical expression for the phase orthogonal output spectral density used to measure the sensing performance. In Sec. IV, we analyze the roles played by the antirotating term and antirotating wave term in weak magnetic sensing, and evaluate the response performance of our weak magnetic sensing scheme to external detection magnetic fields and the suppression of additional noise. In addition, the superiority of this scheme is demonstrated through comparison with previous schemes. The discussion and conclusions are given in Sec. V.

II. SENSING SYSTEM AND HAMILTONIAN

Our system consists of a YIG sphere and a microwave cavity, with the YIG sphere acting as a probe for magnetic field sensing and the output of the microwave cavity acting as a readout for external magnetic field information. The diagrammatic sketch is shown in Fig. 1. In this model, the coupling between the microwave cavity mode and the magnon mode is generated by the magnetic dipole-dipole interaction and the frequency of the magnon mode can be tuned by the external dual frequency modulated field $B_b(t) = B_{b0} + \sum_{i=1,2} B_{bi} \cos(\omega_i t + \phi_i)$, and the two modes are, respectively, pumped by two different semiclassical coherent pump fields. Thus the Hamiltonian of the system reads

$$\begin{aligned} \hat{H} = & \hbar\omega_a \hat{a}^\dagger \hat{a} + \hbar[\omega_m + \sum_{i=1}^2 \lambda_i \omega_i \cos(\omega_i t + \phi_i)] \hat{m}^\dagger \hat{m} + \hbar g (\hat{a} + \hat{a}^\dagger) (\hat{m} + \hat{m}^\dagger) + i\hbar E_d (\hat{m}^\dagger e^{-i\omega_d t} - \hat{m} e^{i\omega_d t}) \\ & + i\hbar E_L (\hat{a}^\dagger e^{-i\omega_L t} - \hat{a} e^{i\omega_L t}) - \hbar \epsilon B_{ex}(t) (\hat{m} + \hat{m}^\dagger). \end{aligned} \quad (1)$$

The first two terms of the Hamiltonian represent the free Hamiltonian of the cavity mode and the magnon mode, where \hat{a} , \hat{m} (\hat{a}^\dagger , \hat{m}^\dagger) are the bosonic annihilation (creation) operators of the cavity mode and magnon mode, ω_a , ω_m are the resonant frequencies of the cavity field and the magnon mode, ω_i , ϕ_i ($i = 1, 2$) denote the two frequencies and phases of the dual frequency modulated bias magnetic field, respectively, and λ_i ($i = 1, 2$) is the coupling coefficient between the dual frequency modulated bias magnetic field and the magnon mode. Due to the bias field, the frequency of the magnon mode of the YIG sphere can be modulated, i.e., $\omega_m = \gamma B_{b0}$, $\lambda_i = \gamma B_{bi} / \omega_i$. The third to the fifth terms are the dipole-dipole

interaction between the cavity field mode and the magnon mode, the classical driving of the cavity field, and the driving of the magnon mode, where $g = \frac{\gamma B_0}{2} \sqrt{5N}$ is the coupling coefficient between the cavity mode and the magnon mode, and B_0 is the amplitude of the microwave field. $E_L = \sqrt{\frac{2P_L \kappa_a}{\hbar\omega_L}}$, ω_L ($E_d = \frac{\gamma B_d}{4} \sqrt{5N}$, ω_d) [44] are the amplitude and frequency of the microwave pump field (magnon mode driving field), P_L represents the input power of the microwave cavity field, and B_d is the magnetic induction intensity of the magnon driving field. According to the experiment, the gyromagnetic ratio $\gamma / 2\pi = 28$ GHz/T [32]. The last term represents the

coupling of the probed magnetic field to the YIG sphere, which can be obtained from the Holstein-Primakoff transformations [52], where $\epsilon = \frac{\gamma}{2}\sqrt{5N}$ is the coupling coefficient between the detected magnetic field and the YIG sphere. It is worth noting that ω_i represents the frequency of the external driving field, and its magnitude is in the range of 10^1 GHz; the value of λ_i depends on the ratio of the product of the external modulation field B_{bi} and the rotational magnetic ratio γ to

the frequency of the modulation field. According to existing experimental conditions, the magnitude of B is 10^0 T, so it is reasonable for λ_i to range from 10^{-1} to 10^0 .

Considering a special unitary transformation operation $\hat{U}(t) = \exp[-i(\omega_L \hat{a}^\dagger \hat{a} + \omega_d \hat{m}^\dagger \hat{m})t] \exp[-i \sum_{i=1}^2 \lambda_i \sin(\omega_i t + \phi_i) \hat{m}^\dagger \hat{m}]$ and the Jacobi-Anger expansions $e^{i\lambda \sin x} = \sum_{m=-\infty}^{\infty} J_m(\lambda) e^{imx}$ [53,54], the Hamiltonian becomes

$$\hat{H}' = \hbar \Delta_a \hat{a}^\dagger \hat{a} + \hbar \Delta_m \hat{m}^\dagger \hat{m} - \hbar \epsilon B_{\text{ex}}(t) (\hat{m} e^{-i\omega_d t} + \hat{m}^\dagger e^{i\omega_d t}) + \hbar (g_1 \hat{m} + g_2 \hat{m}^\dagger) \hat{a} + \hbar (g_1 \hat{m}^\dagger + g_2 \hat{m}) \hat{a}^\dagger + i \hbar E_L (\hat{a}^\dagger - \hat{a}) + i \hbar E_d (\hat{m}^\dagger - \hat{m}), \quad (2)$$

where $\Delta_a = \omega_a - \omega_L$ and $\Delta_m = \omega_m - \omega_d$ are the detunings of the cavity mode and the magnon mode relative to their respective driving field frequencies, and the time-dependent coupling strength g_1 and g_2 can be explicitly given as

$$\begin{aligned} \frac{g_1}{g} &= \sum_{m_{1,2}=-\infty}^{\infty} J_{m_1}(\lambda_1) J_{m_2}(\lambda_2) e^{-i(\omega_L + \omega_d + m_1 \omega_1 + m_2 \omega_2)t - i(m_1 \phi_1 + m_2 \phi_2)}, \\ \frac{g_2}{g} &= \sum_{n_{1,2}=-\infty}^{\infty} J_{n_1}(\lambda_1) J_{n_2}(\lambda_2) e^{-i(\omega_L - \omega_d - n_1 \omega_1 - n_2 \omega_2)t + i(n_1 \phi_1 + n_2 \phi_2)}. \end{aligned} \quad (3)$$

Let us focus on the strong-coupling regime [30], i.e., $\kappa_a, \kappa_m < g \ll \omega_a, \omega_m$, and let $\omega_1 = \omega_d - \omega_L$, $\omega_2 = \omega_L + \omega_d$. If $|(1 - m_1 + m_2)\omega_a + (1 + m_1 + m_2)\omega_d| \ll g$, $|(1 + n_1 - n_2)\omega_a - (1 + n_1 + n_2)\omega_d| \ll g$, the high-frequency oscillation term can be safely neglected, so we can only consider $m_1 = 0$, $m_2 = -1$, $n_1 = -1$, and $n_2 = 0$. Thus one can arrive at the final Hamiltonian as

$$\begin{aligned} \hat{H}_f &= \hbar \Delta_a \hat{a}^\dagger \hat{a} + \hbar \Delta_m \hat{m}^\dagger \hat{m} + \hbar (g_1 \hat{m} e^{i\phi_2} + g_2 \hat{m}^\dagger e^{-i\phi_1}) \hat{a} + \hbar (g_1 \hat{m}^\dagger e^{-i\phi_2} + g_2 \hat{m} e^{i\phi_1}) \hat{a}^\dagger + i \hbar E_L (\hat{a}^\dagger - \hat{a}) \\ &+ i \hbar E_d (\hat{m}^\dagger - \hat{m}) - \hbar \epsilon B_{\text{ex}}(t) (\hat{m} e^{-i\omega_d t} + \hat{m}^\dagger e^{i\omega_d t}), \end{aligned} \quad (4)$$

where the cavity magnetic coupling strength can be simplified as

$$g_1 = g J_0(\lambda_1) J_{-1}(\lambda_2), \quad g_2 = g J_0(\lambda_2) J_{-1}(\lambda_1). \quad (5)$$

Equation (5) indicates that g_1 and g_2 can be adjusted by λ_1 and λ_2 . Since g_1 reflects the dual mode squeezing interaction corresponding to the antirotating wave term, and g_2 reflects the beam-splitter-type interaction corresponding to the rotating wave term, one can freely adjust the ratio of the rotating wave term and the antirotating wave term, which is of great advantage to quantum information processing. In addition, we do not need ultrastrong-coupling or deep-strong-coupling mechanisms for the antirotational wave term, which is also easier to achieve in experiments [42,55].

It is worth emphasizing that the selection of frequencies is essential for achieving the desired interactions and behaviors in this system. The conditions $(\omega_1 = \omega_d - \omega_L)$ and $(\omega_2 = \omega_L + \omega_d)$ are important for eliminating time dependency in the coupling strengths (g_1) and (g_2). These conditions facilitate the use of a special unitary transformation employing the Jacobi-Anger expansion, transforming a time-dependent problem into a time-independent one. By setting $(\omega_1 = \omega_d - \omega_L)$ and $(\omega_2 = \omega_L + \omega_d)$, time-dependent terms in the Hamiltonian are negated, resulting in a time-independent effective Hamiltonian. This simplification is vital for the analytical tractability and comprehension of the system's quantum dynamics. Deviation from these conditions could reintroduce time dependency, complicating the analysis and possibly leading to less efficient mode coupling. This could diminish the effectiveness of the sensing. In practical applications, these conditions dictate the experimental setup, influencing the choice

of frequencies for the applied fields and the design of the cavity and magnon systems to fulfill the required conditions.

III. DYNAMICS OF THE SENSING SYSTEM

For simplicity, in the following, we set $\phi_i = 0$ ($i = 1, 2$). Considering the fluctuations and dissipations, the quantum Langevin equation [56] of the weak-magnetic-field sensing system can be written as

$$\begin{aligned} \dot{\hat{a}} &= -i \Delta_a \hat{a} - \frac{\kappa_a}{2} \hat{a} - i g_1 \hat{m}^\dagger - i g_2 \hat{m} + E_L + \sqrt{\kappa_a} \hat{a}_{\text{in}}(t), \\ \dot{\hat{m}} &= -i \Delta_m \hat{m} - \frac{\kappa_m}{2} \hat{m} - i g_1 \hat{a}^\dagger - i g_2 \hat{a} + E_d + \sqrt{\kappa_m} \hat{m}_{\text{in}}(t) \\ &+ i \epsilon B_{\text{ex}}(t) e^{i\omega_d t}, \end{aligned} \quad (6)$$

where κ_a and κ_m are the dissipations of the cavity field and the magnon mode, respectively, and $\hat{a}_{\text{in}}(t)$ and $\hat{m}_{\text{in}}(t)$ are the input noise operators of the vacuum field cavity mode and the magnetic mode, respectively. These operators are responsible for the stochastic behaviors of the system due to the coupling of the system to its environment. These noise operators satisfy the commutation relationship of bosonic operators and have zero mean values, i.e.,

$$\begin{aligned} \langle \hat{a}_{\text{in}}(t) \hat{a}_{\text{in}}^\dagger(t') \rangle &= (\bar{n}_a + 1) \delta(t - t'), \\ \langle \hat{a}_{\text{in}}^\dagger(t) \hat{a}_{\text{in}}(t') \rangle &= \bar{n}_a \delta(t - t'), \\ \langle \hat{m}_{\text{in}}(t) \hat{m}_{\text{in}}^\dagger(t') \rangle &= (\bar{n}_m + 1) \delta(t - t'), \\ \langle \hat{m}_{\text{in}}^\dagger(t) \hat{m}_{\text{in}}(t') \rangle &= \bar{n}_m \delta(t - t'), \end{aligned} \quad (7)$$

where $\bar{n}_a = [\exp(\hbar \omega_a / k_B T) - 1]^{-1}$ ($\bar{n}_m = [\exp(\hbar \omega_m / k_B T) - 1]^{-1}$) is the thermal occupancy number of the cavity field mode (magnon mode). Based on the strong classical coherent

driving of the system, we can write $\hat{a} = \bar{a} + \delta\hat{a}$, $\hat{m} = \bar{m} + \delta\hat{m}$, and ignore high-order fluctuations. So the Langevin equations for the fluctuation operators read

$$\begin{aligned}\delta\dot{\hat{a}} &= -i\Delta_a\delta\hat{a} - \frac{\kappa_a}{2}\delta\hat{a} - ig_1\delta\hat{m}^\dagger - ig_2\delta\hat{m} + \sqrt{\kappa_a}\hat{a}_{\text{in}}(t), \\ \delta\dot{\hat{m}} &= -i\Delta_m\delta\hat{m} - \frac{\kappa_m}{2}\delta\hat{m} - ig_1\delta\hat{a}^\dagger - ig_2\delta\hat{a} + \sqrt{\kappa_m}\hat{m}_{\text{in}}(t) \\ &\quad + i\epsilon B_{\text{ex}}(t)e^{i\omega_d t}.\end{aligned}\quad (8)$$

To better calculate the phase quadrature component sensing, we rearrange the above equations (8) in the matrix form with the corresponding orthogonal fluctuation operators as

$$\dot{\hat{V}} = C\hat{V} + \hat{V}_{\text{in}}, \quad (9)$$

where $\hat{V} = [\delta\hat{X}_a(t), \delta\hat{P}_a, \delta\hat{X}_m, \delta\hat{P}_m]^T$, $\hat{V}_{\text{in}} = [\sqrt{\kappa_a}\hat{x}_a^{\text{in}}, \sqrt{\kappa_a}\hat{p}_a^{\text{in}}, \sqrt{\kappa_m}\hat{x}_m^{\text{in}}, \sqrt{\kappa_m}\hat{p}_m^{\text{in}}]^T$, and

$$C = \begin{pmatrix} \frac{-\kappa_a}{2} & \Delta_a & 0 & g_2 - g_1 \\ -\Delta_a & \frac{-\kappa_a}{2} & -(g_1 + g_2) & 0 \\ 0 & g_2 - g_1 & \frac{-\kappa_m}{2} & \Delta_m \\ -(g_1 + g_2) & 0 & -\Delta_m & \frac{-\kappa_m}{2} \end{pmatrix}, \quad (10)$$

with $\delta\hat{X}_a = (\hat{a}^\dagger + \hat{a})/\sqrt{2}$, $\delta\hat{P}_a = (\hat{a} - \hat{a}^\dagger)/\sqrt{2}i$, $\delta\hat{X}_m = (\hat{m} + \hat{m}^\dagger)/\sqrt{2}i$, $\delta\hat{P}_m = (\hat{m} - \hat{m}^\dagger)/\sqrt{2}i$, $\hat{x}_a^{\text{in}} = (\hat{a}_{\text{in}}^\dagger + \hat{a}_{\text{in}})/\sqrt{2}$, and $\hat{p}_a^{\text{in}} = (\hat{a}_{\text{in}} - \hat{a}_{\text{in}}^\dagger)/\sqrt{2}i$. It is worth noting that the definition of the quadrature component of the magnon mode has been modified as

$$\begin{aligned}\hat{x}_m^{\text{in}}(t) &= \hat{x}_m^{\text{in}} - \sqrt{\frac{2}{\kappa_m}}\epsilon B_{\text{ex}}(t)\sin(\omega_d t), \\ \hat{p}_m^{\text{in}}(t) &= \hat{p}_m^{\text{in}} + \sqrt{\frac{2}{\kappa_m}}\epsilon B_{\text{ex}}(t)\cos(\omega_d t),\end{aligned}\quad (11)$$

where $\hat{x}_m^{\text{in}} = (\hat{m}_{\text{in}}^\dagger + \hat{m}_{\text{in}})/\sqrt{2}$ and $\hat{p}_m^{\text{in}} = (\hat{m}_{\text{in}} - \hat{m}_{\text{in}}^\dagger)/\sqrt{2}i$ are the quadrature component operators of the magnon mode before correction.

The stability of the system can be guaranteed by the Routh-Hurwitz stability criterion [57], which requires the matrix C satisfying

$$\begin{aligned}H_3 &> 0, H_3H_2 - H_1 > 0, \\ H_3H_2H_1 - (H_1^2 + H_3^2H_0) &> 0,\end{aligned}\quad (12)$$

with

$$\begin{aligned}H_3 &= \kappa_a + \kappa_m, \quad H_2 = 2(g_2^2 - g_1^2) + \Delta_a^2 + \Delta_m^2 + \frac{\kappa_a^2}{4} + \frac{\kappa_m^2}{4} + \kappa_a\kappa_m, \\ H_1 &= -g_1^2\kappa_a + g_2^2\kappa_a + \Delta_m^2\kappa_a - g_1^2\kappa_m + g_2^2\kappa_m + \Delta_a^2\kappa_m + \frac{1}{4}\kappa_a^2\kappa_m + \frac{1}{4}\kappa_a\kappa_m^2, \\ H_0 &= g_1^4 - 2g_1^2g_2^2 + g_2^4 - 2g_1^2\Delta_a\Delta_m - 2g_2^2\Delta_a\Delta_m + \Delta_a^2\Delta_m^2 + \frac{1}{4}\Delta_m^2\kappa_a^2 - \frac{1}{2}g_1^2\kappa_a\kappa_m + \frac{1}{2}g_2^2\kappa_a\kappa_m + \frac{1}{4}\Delta_a^2\kappa_m^2 + \frac{1}{16}\kappa_a^2\kappa_m^2.\end{aligned}\quad (13)$$

Based on the Fourier transform for the operator $\hat{O}(\omega) = \frac{1}{2\pi} \int_{-\infty}^{\infty} dt O(t)e^{i\omega t}$, the fluctuation operator in the time domain can be transferred to the frequency domain; hence, from the input-output relationship $\delta\hat{P}_a^{\text{out}} = \sqrt{\kappa_a}\delta\hat{P}_a - \hat{p}_a^{\text{in}}$, one can obtain the quadrature component of the phase as

$$\delta\hat{P}_a^{\text{out}}(\omega) = M_1(\omega)\hat{x}_m^{\text{in}}(\omega) + M_2(\omega)\hat{p}_m^{\text{in}}(\omega) + M_3(\omega)\hat{x}_a^{\text{in}}(\omega) + M_4(\omega)\hat{p}_a^{\text{in}}(\omega), \quad (14)$$

where $\hat{x}_m^{\text{in}}(\omega) = \hat{x}_m^{\text{in}}(\omega) + \epsilon\sqrt{\frac{1}{2\kappa_m}}i[B_{\text{ex}}(\omega + \omega_d) - B_{\text{ex}}(\omega - \omega_d)]$ and $\hat{p}_m^{\text{in}}(\omega) = \hat{p}_m^{\text{in}}(\omega) + \epsilon\sqrt{\frac{1}{2\kappa_m}}[B_{\text{ex}}(\omega + \omega_d) + B_{\text{ex}}(\omega - \omega_d)]$ are the magnon orthogonal fluctuation operator including the external detected magnetic field, and

$$\begin{aligned}M_1(\omega) &= \frac{\chi_a\chi_m'\sqrt{\kappa_a\kappa_m}\{(g_1 + g_2) + \chi_a\chi_m(g_1 - g_2)[\Delta_a\Delta_m - (g_1 + g_2)^2]\}}{1 + 2\chi_a\chi_m'(g_2^2 - g_1^2) + \chi_a^2\left\{\Delta_a^2 + \chi_m\chi_m'[(g_1^2 - g_2^2)^2 - 2(g_1^2 + g_2^2)]\right\}}, \\ M_2(\omega) &= \frac{\chi_a\chi_m'\sqrt{\kappa_a\kappa_m}[\chi_m(g_1 + g_2)\Delta_m - \chi_a(g_1 - g_2)\Delta_a]}{1 + 2\chi_a\chi_m'(g_2^2 - g_1^2) + \chi_a^2\left\{\Delta_a^2 + \chi_m\chi_m'[(g_1^2 - g_2^2)^2 - 2(g_1^2 + g_2^2)]\right\}}, \\ M_3(\omega) &= \frac{\chi_a^2[\Delta_a - \chi_m\chi_m'(g_1 + g_2)^2\Delta_m]}{1 + 2\chi_a\chi_m'(g_2^2 - g_1^2) + \chi_a^2\left\{\Delta_a^2 + \chi_m\chi_m'[(g_1^2 - g_2^2)^2 - 2(g_1^2 + g_2^2)]\right\}},\end{aligned}$$

$$M_4(\omega) = \frac{1 - \chi_a [2\chi'_m (g_1^2 - g_2^2) + \kappa_a] + \chi_a^2 \{ \Delta_a^2 + \chi'_m \chi_m (g_1^2 - g_2^2) - \chi'_m [2\chi_m (g_1^2 + g_2^2) \Delta_a \Delta_m + (g_2^2 - g_1^2) \kappa_a] \}}{1 + 2\chi_a \chi'_m (g_2^2 - g_1^2) + \chi_a^2 \{ \Delta_a^2 + \chi_m \chi'_m [(g_1^2 - g_2^2)^2 - 2(g_1^2 + g_2^2)] \}}, \quad (15)$$

with $\chi_a(\omega) = \frac{1}{\kappa_a/2 - i\omega}$ and $\chi_m(\omega) = \frac{1}{\kappa_m/2 - i\omega}$ being the susceptibility of the cavity field and the magnon mode, and $\chi'_m = \frac{1}{1/\chi_m + \Delta_a^2}$ denoting the effective susceptibility of the magnon mode.

To achieve weak-magnetic-field sensing, we need to use a homodyne detection device to detect the phase output symmetrical spectrum density, defined as [58]

$$Y_{\text{out}}(\omega) = \frac{1}{2} \int d\omega' e^{i(\omega+\omega')t} \langle \delta P_a^{\text{out}}(\omega) \delta P_a^{\text{out}}(\omega') + \delta P_a^{\text{out}}(\omega') \delta P_a^{\text{out}}(\omega) \rangle. \quad (16)$$

According to Eq. (7), the cavity field phase output spectrum density of the system can be written as

$$Y_{\text{out}}(\omega) = (\bar{n}_a + \frac{1}{2}) [|M_4(\omega)|^2] + |M_1(\omega)|^2 [(\bar{n}_m + \frac{1}{2}) + S_{B_{\text{ex}}}(\omega)], \quad (17)$$

where $S_{B_{\text{ex}}}$ is the signal spectral density of the external magnetic field corresponding to the magnon mode amplitude orthogonal component, respectively. From the expression of the output spectrum, it can be seen that the first term represents the contribution of the microwave cavity field, while the second term represent the contribution of the YIG probe and the detected magnetic field signal. Next, in order to better measure the performance of weak-magnetic-field sensing, we define

$$R_B(\omega) = \partial Y_{\text{out}}(\omega) / \partial S_{B_{\text{ex}}}(\omega) = |M_1(\omega)|^2, \quad (18)$$

$$\begin{aligned} N_{\text{ad}}(\omega) &= \left(\bar{n}_a + \frac{1}{2} \right) \frac{[|M_4(\omega)|^2]}{\partial Y_{\text{out}}(\omega) / \partial S_{B_{\text{ex}}}(\omega)} \\ &= \left(\bar{n}_a + \frac{1}{2} \right) \frac{[|M_4(\omega)|^2]}{|M_1(\omega)|^2}, \end{aligned} \quad (19)$$

which represent the response to external magnetic signals and the additional noise including cavity field thermal noise and quantum noise in weak-magnetic-field sensing, respectively. From Eq. (17), one can see that $R_B(\omega) > 1$ indicates the signal amplification, and the smaller the additional noise $N_{\text{ad}}(\omega)$ of the system is, the easier it is to detect the signal of the external magnetic field. In addition, when $N_{\text{ad}}(\omega) < 1/2$, we say that additional noise is below the SQL [58]. Therefore, reducing the additional noise below the SQL will improve the sensitivity of weak magnetic sensing. In this sense, we will not consider the specific expression of the detected magnetic field signal spectrum, but focus on reducing the additional noise and enhancing the response.

IV. WEAK-MAGNETIC-FIELD SENSING

In this section, we provide numerical results of the performance of our weak magnetic sensing scheme. Our scheme can greatly relax the requirements for cavity magnetic coupling strength and achieve additional noise suppression of the same order of magnitude without dual frequency modulation under the super-strong-coupling mechanism or deep-strong-coupling mechanism. The scheme without dual frequency

modulation was recently proposed by Ebrahimi *et al.* [7]. Therefore, we reproduced some of their results and compared them with our scheme. In addition, we have set the following feasible experimental parameters [30]: $\omega_m/2\pi = 37.5$ GHz, $g = 10^{-2}\omega_m$, $\Delta_a = \Delta_m = 0$, $\kappa_m/2\pi = 15$ MHz, $\kappa_a/2\pi = 33$ MHz.

First, we would like to study how the rotating wave interaction and antirotating wave interaction affect weak-magnetic-field sensing. We set $\Delta_a = \Delta_m = 0$, which can be achieved by adjusting the bias field and the frequency of the external driving microwave field. This setting can decouple the two orthogonal components of the magnon mode and the orthogonal components of the cavity field, thereby improving the sensitivity of the measurement. We plot the additional noise of weak-magnetic-field sensing and the response to external magnetic signals versus the frequency in Fig. 2. The red solid line corresponds to the presence of the only rotating wave term, and the blue dashed line indicates the only antirotating wave term that is present. Figure 2(a) shows that neither type of interaction alone can increase the system's response to external magnetic field signals since the curves are below 10^0 . Figure 2(b) shows that under resonance conditions ($\omega \approx 0$), the additional noise suppression level of the rotating wave term is greater than that of the nonrotating wave term, and it also has great noise suppression performance in the nonresonant region. This result indicates that the interaction of rotating wave terms is beneficial for improving the sensitivity of detection, which can be understood as the result of a beam-splitter-type interaction between the magnon and the cavity photon. That is, when the external magnetic field affects the magnon, coherent energy exchange occurs between the magnon and the photon, which is more conducive to optical field readout and thus improves sensitivity.

In Fig. 3(a), we plot the response of the system with additional noise under different λ_2/λ_1 with both the rotating and nonrotating wave terms present. The red curve corresponds to $\lambda_2 = \lambda_1$, namely, the rotating wave term and the nonrotating wave term have the same weight in the Hamiltonian. One can find that with the relative weight (λ_2/λ_1) of the nonrotating wave term increasing, the response of the system is correspondingly improved in the resonance region. This result indicates that a single parametric amplification interaction (nonrotating wave term) cannot amplify the signal to be detected, and it must coexist with the beam-splitter-type interaction (rotating wave term). Figure 3(b) shows the additional noise of the system with different λ_2/λ_1 . At the low environment temperature of 50 mK, implying the low-environment thermal noise, it can be found that under resonance condition ($\omega \approx 0$), the best suppression of additional noise is not under the condition of $\lambda_2 = \lambda_1$, but at $\lambda_2 = 0.95\lambda_1$. At $\omega \approx 0.33\kappa_m$, there is a valley region where the additional noise suppression effect is one order of magnitude stronger than the case of

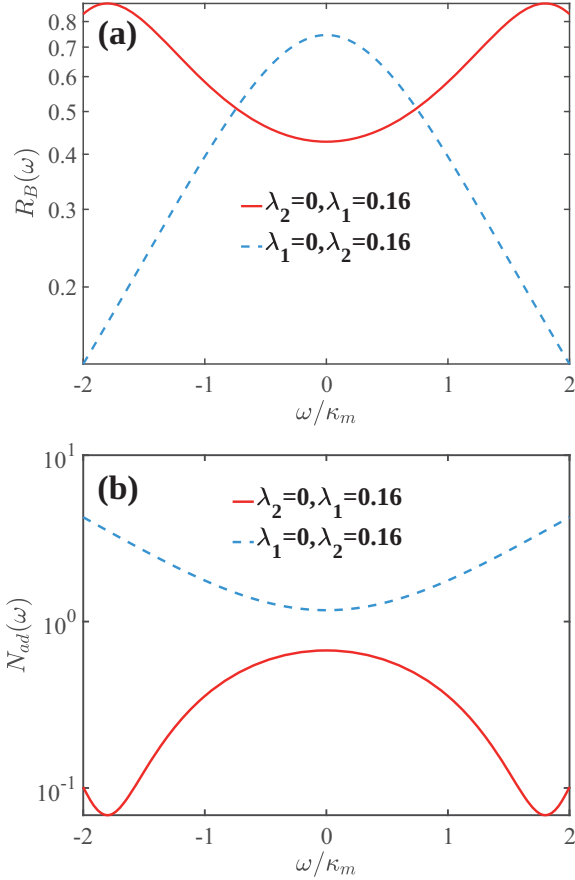


FIG. 2. (a) The response R_B of the system as a function of the normalized frequency ω/κ_m . (b) The additional noise N_{ad} as a function of normalized frequency ω/κ_m . The red solid line represents the case of only rotating wave term interaction, while the blue dashed line represents the case of only antirotating wave term interaction. The experimental parameters related to (a) and (b) are $\omega_m/2\pi = 37.5$ GHz, $g = 10^{-2}\omega_m$, $\Delta_a = \Delta_m = 0$, $\kappa_m/2\pi = 15$ MHz, and $\kappa_a/2\pi = 33$ MHz. In addition, we set the environment temperature to 50 mK, which is unaffected by thermal noise.

$\lambda_2 = \lambda_1$. In addition, for $\lambda_2/\lambda_1 = 0.3, 0.6$, the suppression effect is not apparent, even though both have a suppression valley.

To emphasize the performance of this sensor in the presence of environmental thermal noise, in Fig. 4(a), we study the additional noise of the system versus the normalized frequency at room temperature ($T = 300$ K). One can find that at $\lambda_2 = 0.95\lambda_1$, the additional noise can still be suppressed below the SQL [$N_{ad}(\omega) < \frac{1}{2}$] in the $\omega \approx 0$. Especially in Fig. 4(b), we plot the curves of the additional noise with temperature, which indicates that in a wide temperature range, the additional noise can be suppressed below the SQL. In particular, our scheme can extremely strongly suppress the additional noise under the strong-coupling regime instead of the ultrastrong or deep-strong coupling required for the antirotating wave term interaction.

Next, we compared the additional noise suppression performance of our scheme with the scheme without dual frequency bias field modulation. In Fig. 5(a), the red solid line represents the scheme without dual frequency

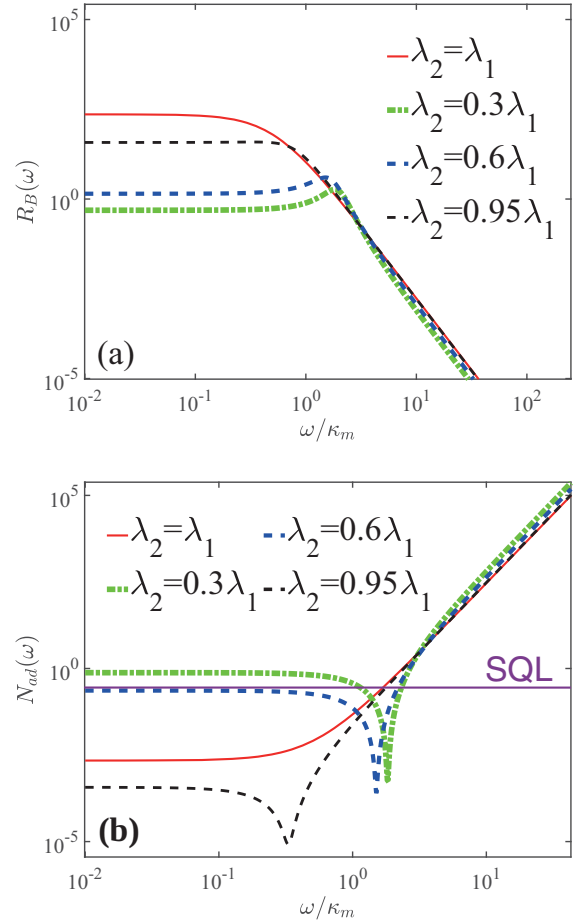


FIG. 3. (a) The response R_B of the system as a function of the normalized frequency ω/κ_m , with logarithmic scale on the x axis. (b) The additional noise N_{ad} as a function of normalized frequency ω/κ_m , with logarithmic scale on the x axis. λ_2 is set to 0, $0.3\lambda_1$, $0.6\lambda_1$, and $0.95\lambda_1$. Other parameters are $\omega_m/2\pi = 37.5$ GHz, $g = 10^{-2}\omega_m$, $\lambda_1 = 0.16$, $\Delta_a = \Delta_m = 0$, $\kappa_m/2\pi = 15$ MHz, and $\kappa_a/2\pi = 33$ MHz. In addition, we set the environment temperature to 50 mK, which is almost unaffected by thermal noise.

modulation, and the blue dashed line represents the additional noise suppression result of our scheme. It can be seen that the red solid line does not have a good additional noise suppression effect, which is the same as the result of Ref. [7]. However, our scheme can achieve the additional noise suppression effect in the resonance region that exceeds the scheme without dual frequency modulation by nearly five orders of magnitude.

Before the end, we would like to emphasize that dual frequency bias field driving is a key to our scheme. Next, we will pay attention to the case of the *ultrastrong-* or *deep-strong-* coupling scheme. The zero-detuning conditions ($\Delta_m = \Delta_a = 0$) for the ultrastrong-coupling scheme are given as [7]

$$R_{B2}(\omega) = 4\kappa_a^2\kappa_m^2C \left| \frac{\chi_{m1}(\omega)}{2i\omega + \kappa_a} \right|^2, \quad (20)$$

$$N_{ad2}(\omega) = \frac{\left| 1 + \frac{2\kappa_a}{2i\omega + \kappa_a} \right|^2 (\bar{n}_a + \frac{1}{2})}{4\kappa_a^2\kappa_m^2C \left| \frac{\chi_{m1}(\omega)}{2i\omega + \kappa_a} \right|^2}, \quad (21)$$

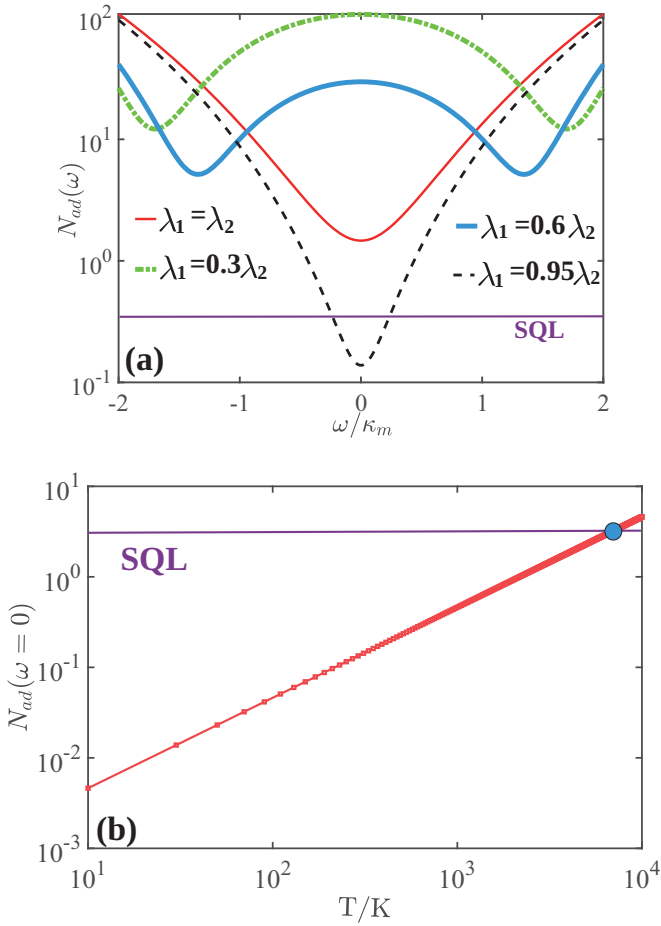


FIG. 4. (a) The additional noise N_{ad} as a function of normalized frequency ω/κ_m . Unlike Fig. 3(b), we set the temperature to room temperature, i.e., $T = 300$ K. (b) The additional noise $N_{ad}(\omega = 0)$ as a function of temperature T . The purple solid line represents the SQL. The other experimental parameters related to (a) and (b) are $\omega_m/2\pi = 37.5$ GHz, $g = 10^{-2}\omega_m$, $\lambda_1 = 0.16$, $\Delta_a = \Delta_m = 0$, $\kappa_m/2\pi = 15$ MHz, and $\kappa_a/2\pi = 33$ MHz.

where $\chi_{m1}(\omega) = \frac{1}{\kappa_m/2 + i\omega}$ is the susceptibility, and C is the electromagnetic cooperativity, with a range of 1–1000. In Fig. 5(b), we compare our scheme with the scheme under the super-strong-coupling mechanism. It can be seen that our ability to suppress additional noise can even reach the level of the ultrastrong-coupling scheme with extremely high electromagnetic cooperativity. Specifically, in Fig. 5(b), one can find that the noise suppression effect of our scheme near $\omega \approx 0$ is significantly stronger than that of $C = 10, 100$. Moreover, our scheme can achieve noise suppression of the same order of magnitude under the condition of $C = 1000$, as shown in the inset in Fig. 5(b). When $\omega \approx 0$, the additional noise corresponding to the green dashed line is 0.0002, and our scheme can achieve 0.0004. This demonstrates the potential of our scheme to achieve similar noise suppression capabilities as the ultrastrong-coupling scheme under a strong-coupling mechanism without any parameter adjustments. The comparison in Fig. 5(b) indicates that our scheme can achieve high sensitivity without the necessity of experimental conditions associated with an ultrastrong-coupling mechanism. Of

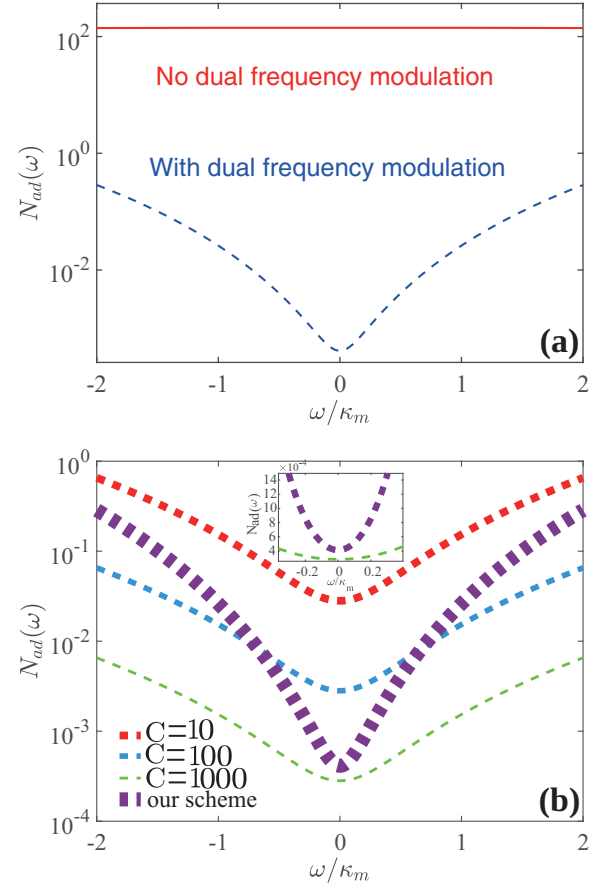


FIG. 5. (a) The additional noise N_{ad} of the system is taken as a function of the normalized frequency ω/κ_m . The blue dashed line represents the presence of a dual frequency modulated magnetic field; the red solid line represents the absence of a dual frequency modulated magnetic field. (b) The additional noise N_{ad} as a function of normalized frequency ω/κ_m under different electromagnetic cooperativity C . Specifically, the red, green, and blue dashes represent the corresponding cases of $C = 10$, $C = 100$, and $C = 1000$ in the ultrastrong-coupling mechanism scheme. The purple dashed line represents our dual frequency modulation bias field scheme. The other experimental parameters related to (a) and (b) are $\omega_m/2\pi = 37.5$ GHz, $g = 10^{-2}\omega_m$, $\lambda_1 = 0.16$, $\lambda_2 = 0.95\lambda_1$, $\Delta_a = \Delta_m = 0$, $\kappa_m/2\pi = 15$ MHz, $\kappa_a/2\pi = 33$ MHz, and $T = 50$ mK.

course, suppose our scheme can be implemented for magnetic field sensing under the ultrastrong-coupling mechanism. In that case, it is natural that the sensitivity and the ability of signal amplification will be further enhanced. This sufficiently demonstrates the superiority of our scheme.

V. DISCUSSION AND CONCLUSIONS

In summary, we proposed a scheme for weak-magnetic-field sensing using dual frequency bias field modulation. The introduction of the dual bias field modulation can adjust the proportion of the rotating and the antirotating wave-type interaction in the weak-magnetic-field sensing system, which help to reveal the crucial roles of the two types of interactions played in the weak-magnetic-field sensing. It is found that

the antirotating wave term can amplify the magnon mode signal, but this amplification effect must coexist with the rotating wave term. In addition, the distinct advantage is that our scheme can achieve a more sensitive and temperature-robust weak-magnetic-field sensing with additional noise, but it does not require an ultrastrong- or a deep-strong-coupling mechanism. In this sense, it reduces the difficulty of experimental implementation. In addition, we compared our scheme with previous schemes that required ultrastrong-coupling or deep-strong-coupling mechanisms and found that in terms of additional noise suppression, our scheme can achieve the additional noise suppression of the same order of magnitude as the previous scheme. This indicates that we can not only relax the experimental conditions, but also have no decrease in sensitivity. Therefore, it can be said that

our scheme achieves highly sensitive weak-magnetic-field sensing. Moreover, although we have achieved the temperature robustness of the additional noise, the thermal noise of the magnon mode is a significant problem and we will study how to reduce the thermal noise of the magnon in the future.

ACKNOWLEDGMENTS

This work was supported by the National Natural Science Foundation of China under Grants No. 12175029, No. 12011530014, and No. 11775040, and the Key Research and Development Project of Liaoning Province, under Grant No. 2020JH2/10500003.

-
- [1] J. F. Barry, R. A. Irion, M. H. Steinecker, D. K. Freeman, J. J. Kedziora, R. G. Wilcox, and D. A. Braje, Ferrimagnetic oscillator magnetometer, *Phys. Rev. Appl.* **19**, 044044 (2023).
- [2] W.-Z. Zhang, L.-B. Chen, J. Cheng, and Y.-F. Jiang, Quantum-correlation-enhanced weak-field detection in an optomechanical system, *Phys. Rev. A* **99**, 063811 (2019).
- [3] Y. Cao and P. Yan, Exceptional magnetic sensitivity of \mathcal{PT} -symmetric cavity magnon polaritons, *Phys. Rev. B* **99**, 214415 (2019).
- [4] S. Forstner, S. Prams, J. Knittel, E. D. van Ooijen, J. D. Swaim, G. I. Harris, A. Szorkovszky, W. P. Bowen, and H. Rubinsztein-Dunlop, Cavity optomechanical magnetometer, *Phys. Rev. Lett.* **108**, 120801 (2012).
- [5] S. Forstner, E. Sheridan, J. Knittel, C. L. Humphreys, G. A. Brawley, H. Rubinsztein-Dunlop, and W. P. Bowen, Ultrasensitive optomechanical magnetometry, *Adv. Mater.* **26**, 6348 (2014).
- [6] B.-B. Li, J. Bílek, U. B. Hoff, L. S. Madsen, S. Forstner, V. Prakash, C. Schäfermeier, T. Gehring, W. P. Bowen, and U. L. Andersen, Quantum enhanced optomechanical magnetometry, *Optica* **5**, 850 (2018).
- [7] M. S. Ebrahimi, A. Motazedifard, and M. B. Harouni, Single-quadrature quantum magnetometry in cavity electromagnonics, *Phys. Rev. A* **103**, 062605 (2021).
- [8] R. Stolz, M. Schmelz, V. Zakosarenko, C. Foley, K. Tanabe, X. Xie, and R. L. Fagaly, Superconducting sensors and methods in geophysical applications, *Supercond. Sci. Technol.* **34**, 033001 (2021).
- [9] D. Murzin, D. J. Mapps, K. Levada, V. Belyaev, A. Omelyanchik, L. Panina, and V. Rodionova, Ultrasensitive magnetic field sensors for biomedical applications, *Sensors* **20**, 1569 (2020).
- [10] K.-M. C. Fu, G. Z. Iwata, A. Wickenbrock, and D. Budker, Sensitive magnetometry in challenging environments, *AVS Quantum Sci.* **2**, 044702 (2020).
- [11] P.-H. Chu, Y. J. Kim, and I. Savukov, Search for an axion-induced oscillating electric dipole moment for electrons using atomic magnetometers, *Phys. Rev. D* **99**, 075031 (2019).
- [12] S. Keenan, C. Pegrum, M. Gali Labarias, and E. E. Mitchell, Determining the temperature-dependent London penetration depth in HTS thin films and its effect on SQUID performance, *Appl. Phys. Lett.* **119**, 142601 (2021).
- [13] X. Zhang, J. Hu, and N. Zhao, Stable atomic magnetometer in parity-time symmetry broken phase, *Phys. Rev. Lett.* **130**, 023201 (2023).
- [14] I. Fescenko, A. Laraoui, J. Smits, N. Mosavian, P. Kehayias, J. Seto, L. Bougas, A. Jarmola, and V. M. Acosta, Diamond magnetic microscopy of malarial hemozoin nanocrystals, *Phys. Rev. Appl.* **11**, 034029 (2019).
- [15] A. A. Clerk, M. H. Devoret, S. M. Girvin, F. Marquardt, and R. J. Schoelkopf, Introduction to quantum noise, measurement, and amplification, *Rev. Mod. Phys.* **82**, 1155 (2010).
- [16] F. Bariani, H. Seok, S. Singh, M. Vengalattore, and P. Meystre, Atom-based coherent quantum-noise cancellation in optomechanics, *Phys. Rev. A* **92**, 043817 (2015).
- [17] S. K. Singh, M. Mazaheri, J.-X. Peng, A. Sohail, M. Khalid, and M. Asjad, Enhanced weak force sensing based on atom-based coherent quantum noise cancellation in a hybrid cavity optomechanical system, *Front. Phys.* **11**, 1142452 (2023).
- [18] A. Motazedifard, F. Bemani, M. H. Naderi, R. Roknizadeh, and D. Vitali, Force sensing based on coherent quantum noise cancellation in a hybrid optomechanical cavity with squeezed-vacuum injection, *New J. Phys.* **18**, 073040 (2016).
- [19] C. B. Møller, R. A. Thomas, G. Vasilakis, E. Zeuthen, Y. Tsaturyan, M. Balabas, K. Jensen, A. Schliesser, K. Hammerer, and E. S. Polzik, Quantum back-action-evading measurement of motion in a negative mass reference frame, *Nature (London)* **547**, 191 (2017).
- [20] H. Allahverdi, A. Motazedifard, A. Dalafi, D. Vitali, and M. H. Naderi, Homodyne coherent quantum noise cancellation in a hybrid optomechanical force sensor, *Phys. Rev. A* **106**, 023107 (2022).
- [21] M. H. Wimmer, D. Steinmeyer, K. Hammerer, and M. Heurs, Coherent cancellation of backaction noise in optomechanical force measurements, *Phys. Rev. A* **89**, 053836 (2014).
- [22] W.-Z. Zhang, Y. Han, B. Xiong, and L. Zhou, Optomechanical force sensor in a non-Markovian regime, *New J. Phys.* **19**, 083022 (2017).
- [23] V. Peano, H. G. L. Schwefel, C. Marquardt, and F. Marquardt, Intracavity squeezing can enhance quantum-limited

- optomechanical position detection through deamplification, *Phys. Rev. Lett.* **115**, 243603 (2015).
- [24] W. Zhao, S.-D. Zhang, A. Miranowicz, and H. Jing, Weak-force sensing with squeezed optomechanics, *Sci. China Math.* **63**, 1 (2020).
- [25] J. Aasi, J. Abadie, B. Abbott, R. Abbott, T. Abbott, M. Abernathy, C. Adams, T. Adams, P. Addesso, R. Adhikari *et al.*, Enhanced sensitivity of the ligo gravitational wave detector by using squeezed states of light, *Nat. Photon.* **7**, 613 (2013).
- [26] S. E. Dwyer, G. L. Mansell, and L. McCuller, Squeezing in gravitational wave detectors, *Galaxies* **10**, 46 (2022).
- [27] F. Meylahn, B. Willke, and H. Vahlbruch, Squeezed states of light for future gravitational wave detectors at a wavelength of 1550 nm, *Phys. Rev. Lett.* **129**, 121103 (2022).
- [28] M. Aspelmeyer, T. J. Kippenberg, and F. Marquardt, Cavity optomechanics, *Rev. Mod. Phys.* **86**, 1391 (2014).
- [29] X. Xu and J. M. Taylor, Squeezing in a coupled two-mode optomechanical system for force sensing below the standard quantum limit, *Phys. Rev. A* **90**, 043848 (2014).
- [30] X. Zhang, C.-L. Zou, L. Jiang, and H. X. Tang, Strongly coupled magnons and cavity microwave photons, *Phys. Rev. Lett.* **113**, 156401 (2014).
- [31] B. Z. Rameshti, S. V. Kusminskiy, J. A. Haigh, K. Usami, D. Lachance-Quirion, Y. Nakamura, C.-M. Hu, H. X. Tang, G. E. Bauer, and Y. M. Blanter, Cavity magnonics, *Phys. Rep.* **979**, 1 (2022).
- [32] X. Zhang, C.-L. Zou, L. Jiang, and H. X. Tang, Cavity magnomechanics, *Sci. Adv.* **2**, e1501286 (2016).
- [33] D. Lachance-Quirion, Y. Tabuchi, A. Gloppe, K. Usami, and Y. Nakamura, Hybrid quantum systems based on magnonics, *Appl. Phys. Express* **12**, 070101 (2019).
- [34] H. Y. Yuan, P. Yan, S. Zheng, Q. Y. He, K. Xia, and M.-H. Yung, Steady Bell state generation via magnon-photon coupling, *Phys. Rev. Lett.* **124**, 053602 (2020).
- [35] O. O. Soykal and M. E. Flatté, Strong field interactions between a nanomagnet and a photonic cavity, *Phys. Rev. Lett.* **104**, 077202 (2010).
- [36] C. Kittel, Interaction of spin waves and ultrasonic waves in ferromagnetic crystals, *Phys. Rev.* **110**, 836 (1958).
- [37] M. Goryachev, W. G. Farr, D. L. Creedon, Y. Fan, M. Kostylev, and M. E. Tobar, High-cooperativity cavity QED with magnons at microwave frequencies, *Phys. Rev. Appl.* **2**, 054002 (2014).
- [38] S. Sharma, Y. M. Blanter, and G. E. W. Bauer, Light scattering by magnons in whispering gallery mode cavities, *Phys. Rev. B* **96**, 094412 (2017).
- [39] H. Huebl, C. W. Zollitsch, J. Lotze, F. Hocke, M. Greifenstein, A. Marx, R. Gross, and S. T. B. Goennenwein, High cooperativity in coupled microwave resonator ferrimagnetic insulator hybrids, *Phys. Rev. Lett.* **111**, 127003 (2013).
- [40] Y. Tabuchi, S. Ishino, T. Ishikawa, R. Yamazaki, K. Usami, and Y. Nakamura, Hybridizing ferromagnetic magnons and microwave photons in the quantum limit, *Phys. Rev. Lett.* **113**, 083603 (2014).
- [41] J. Bourhill, N. Kostylev, M. Goryachev, D. L. Creedon, and M. E. Tobar, Ultrahigh cooperativity interactions between magnons and resonant photons in a YIG sphere, *Phys. Rev. B* **93**, 144420 (2016).
- [42] N. Kostylev, M. Goryachev, and M. E. Tobar, Superstrong coupling of a microwave cavity to yttrium iron garnet magnons, *Appl. Phys. Lett.* **108**, 062402 (2016).
- [43] F.-X. Sun, S.-S. Zheng, Y. Xiao, Q. Gong, Q. He, and K. Xia, Remote generation of magnon Schrödinger cat state via magnon-photon entanglement, *Phys. Rev. Lett.* **127**, 087203 (2021).
- [44] J. Li, S.-Y. Zhu, and G. S. Agarwal, Magnon-photon-phonon entanglement in cavity magnomechanics, *Phys. Rev. Lett.* **121**, 203601 (2018).
- [45] W. Zhang, T. Wang, X. Han, S. Zhang, and H.-F. Wang, Quantum entanglement and one-way steering in a cavity magnomechanical system via a squeezed vacuum field, *Opt. Express* **30**, 10969 (2022).
- [46] Z.-B. Yang, J.-S. Liu, H. Jin, Q.-H. Zhu, A.-D. Zhu, H.-Y. Liu, Y. Ming, and R.-C. Yang, Entanglement enhanced by Kerr nonlinearity in a cavity-optomagnonics system, *Opt. Express* **28**, 31862 (2020).
- [47] B. Hussain, S. Qamar, and M. Irfan, Entanglement enhancement in cavity magnomechanics by an optical parametric amplifier, *Phys. Rev. A* **105**, 063704 (2022).
- [48] J. M. P. Nair and G. S. Agarwal, Deterministic quantum entanglement between macroscopic ferrite samples, *Appl. Phys. Lett.* **117**, 084001 (2020).
- [49] Z.-X. Liu, H. Xiong, and Y. Wu, Magnon blockade in a hybrid ferromagnet-superconductor quantum system, *Phys. Rev. B* **100**, 134421 (2019).
- [50] C. Zhao, X. Li, S. Chao, R. Peng, C. Li, and L. Zhou, Simultaneous blockade of a photon, phonon, and magnon induced by a two-level atom, *Phys. Rev. A* **101**, 063838 (2020).
- [51] C. A. Potts, Y. Huang, V. A. S. V. Bittencourt, S. Viola Kusminskiy, and J. P. Davis, Dynamical backaction evading magnomechanics, *Phys. Rev. B* **107**, L140405 (2023).
- [52] T. Holstein and H. Primakoff, Field dependence of the intrinsic domain magnetization of a ferromagnet, *Phys. Rev.* **58**, 1098 (1940).
- [53] S.-L. Chao, D.-W. Wang, Z. Yang, C.-S. Zhao, R. Peng, and L. Zhou, Backaction evading and amplification of weak force signal in an optomechanical system, *Annal. Phys.* **534**, 2100421 (2022).
- [54] S.-L. Chao, Z. Yang, C.-S. Zhao, R. Peng, and L. Zhou, Force sensing in a dual-mode optomechanical system with linear-quadratic coupling and modulated photon hopping, *Opt. Lett.* **46**, 3075 (2021).
- [55] N. Hu and H. Tan, Two-tone modulated cavity electromagnonics, [arXiv:2305.10653](https://arxiv.org/abs/2305.10653).
- [56] R. Benguria and M. Kac, Quantum Langevin equation, *Phys. Rev. Lett.* **46**, 1 (1981).
- [57] E. X. DeJesus and C. Kaufman, Routh-Hurwitz criterion in the examination of eigenvalues of a system of nonlinear ordinary differential equations, *Phys. Rev. A* **35**, 5288 (1987).
- [58] A. Motazedifard, A. Dalafi, F. Bemani, and M. H. Naderi, Force sensing in hybrid Bose-Einstein-condensate optomechanics based on parametric amplification, *Phys. Rev. A* **100**, 023815 (2019).